

Radial-momentum-resolved measurement of the tunneling ionization time in attoclock experimentsMiao Yu,¹ Yueming Zhou^{1,*}, Kun Liu,¹ Kunlong Liu,¹ Min Li,¹ and Peixiang Lu^{1,2}¹*School of Physics and Wuhan National Laboratory for Optoelectronics,
Huazhong University of Science and Technology, Wuhan 430074, China*²*Optics Valley Laboratory, Hubei 430074, China*

(Received 20 June 2022; accepted 24 October 2022; published 3 November 2022)

We studied the tunneling ionization time in the elliptically polarized laser field with the recently proposed phase-of-the-phase spectroscopy, wherein a weak linearly polarized second-harmonic field was introduced to the attoclock frame. By monitoring the oscillation of the photoelectron yield with the relative phase between the two fields, the ionization time of the photoelectrons can be determined without any effort on handling the Coulomb interaction between the escaping electron and the parent ion. This advantage enables us to resolve the ionization time in the full photoelectron momentum distribution. By solving the time-dependent Schrödinger equation, we showed that the ionization time depends on the radial momentum of photoelectron. The photoelectron with larger radial momentum ionizes earlier at the emission angle before the most probable emission angle, while this radial-momentum dependence is reversed at the emission angle after the most probable emission angle. These results are confirmed by our experiments.

DOI: [10.1103/PhysRevA.106.053106](https://doi.org/10.1103/PhysRevA.106.053106)**I. INTRODUCTION**

Tunneling is a fundamental process in quantum mechanics. The question of how long it takes a particle to tunnel through a barrier has attracted extensive attention since the birth of quantum mechanics [1–5]. The answer is not only important for understanding this fundamental process but also has wide-ranging practical implications for various strong-field phenomena triggered by tunneling ionization, such as high-harmonic generation spectroscopy [6], laser-induced diffraction [7–9], and photoelectron holography [10–14]. Advances in the ultrafast laser technology have opened up the opportunity to experimentally resolve the attosecond electron dynamics of tunneling. Among them, the attoclock is a powerful technique to measure ionization time [15], where an elliptically polarized laser pulse is used to map the ionization time of the photoelectron to its emission angle in the laser polarization plane. The tunneling time delay is extracted from the measured offset angle of the maximum of the photoelectron momentum distribution (PEMD) with respect to the minor axis of the elliptically polarized laser field [16].

Typically, in the attoclock experiments only the most probable electron emission angle, which is obtained by integrating the radial momentum, is analyzed [16–31]. The measured ionization time is a single value for this most probable emission angle. Actually, the ionization time in the attoclock experiment is much more complex than this single value. It has been proposed that the tunneling time delay is probabilistic, rather than a deterministic quantity [19,20]. Moreover, it has been demonstrated that the angular distribution in the attoclock experiments sensitively depends on the radial momentum of

the photoelectrons [32–36]. It implies that the ionization time of electrons along the same emitting angle may vary with the radial momentum of photoelectron, which raises concerns about the accuracy of the single time constructed from a single value of the offset angle. Therefore it is essential to extract the ionization time from the full momentum distribution, which contains much more information regarding the tunneling process.

In previous attoclock experiments, the critical task is the determination of deflection angle of the photoelectron induced by the long-range Coulomb potential, which is usually obtained from classical trajectories of escaping electron. Calculation of this deflection angle requires accurate information of the laser parameters (such as laser intensity, ellipticity, etc.), and even worse, it depends on the initial conditions of the trajectories, such as the tunneling exit and the initial velocity, which are model dependent. This is the origin of the controversy on the ionization time for the most probable emission angle in previous attoclock experiments [21,25,37]. Regarding the radial-momentum-resolved ionization time, it is more difficult to handle the effect of the Coulomb interaction, and thus it is more challenging to achieve the radial-momentum-resolved ionization time with the previous attoclock. Recently, we introduced the phase-of-the-phase spectroscopy [38–42] to the attoclock experiment to overcome this difficulty [43]. In our scheme, instead of extracting the ionization time from the offset angle of the PEMDs, a weak second-harmonic (SH) field is used to modulate the tunneling current produced by the fundamental field. By monitoring the response of the photoelectron yield at each place in the PEMDs to the relative phase between the fundamental and the SH fields, the instant of tunneling ionization of the photoelectrons is determined unambiguously. Our method is free from modeling the Coulomb effect on the escaping photoelectron, and thus

*zhouymhust@hust.edu.cn

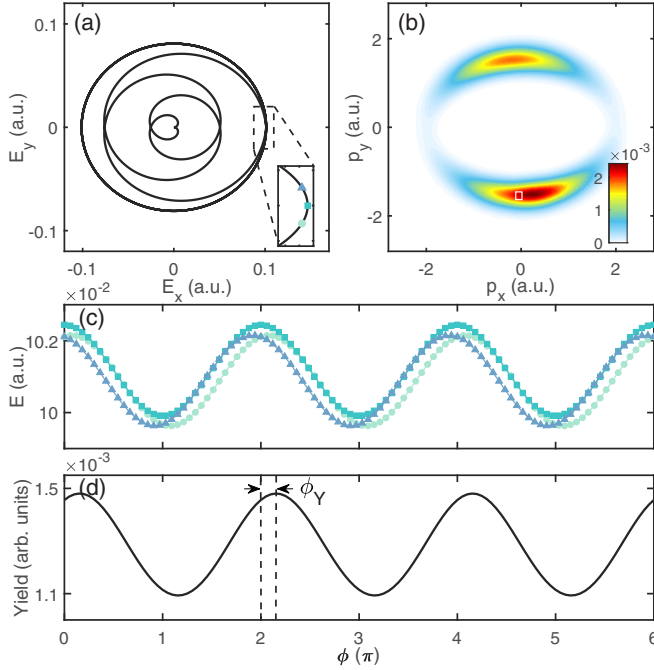


FIG. 1. (a) Electric field of the elliptically polarized laser pulse. (b) The PEMD from tunneling ionization by the elliptically polarized laser pulse. (c) The synthesized electric field strength with respect to the relative phase at three instants, as marked by the corresponding symbols in (a). (d) For a given momentum \mathbf{p} [as indicated by the white box in (b)], the photoelectron yield oscillates with the relative phase. The optimal phase ϕ_Y indicates the phase maximizing the ionization rate (i.e., the phase of the phase).

previous debates on identifying Coulomb-induced deflection angle are avoided. This superiority enables us to determine the ionization time of the photoelectron in the full momentum distribution in the attoclock experiments. In this paper we employ this scheme to determine the radial-momentum-resolved tunneling ionization time. Our results show that the ionization time depends on the radial momentum of the photoelectron, and this radial-momentum dependence of the ionization time depends on the emission angle of the photoelectron.

II. METHODS

Figure 1 illustrates the scheme of our method. A strong elliptically polarized laser field [Fig. 1(a)] triggers tunneling ionization. The corresponding PEMD is shown in Fig. 1(b). A weak SH field is introduced to perturb the fundamental field. The synthesized electric field is written as [atomic units (a.u.) are used unless stated otherwise]

$$\mathbf{E}(t, \phi) = [E_{800} \cos(\omega t) + E_{400} \cos(2\omega t + \phi)]\mathbf{e}_x + \epsilon E_{800} \sin(\omega t)\mathbf{e}_y, \quad (1)$$

where ω is the frequency of the fundamental 800-nm field, ϵ is the ellipticity of the fundamental pulse, \mathbf{e}_x and \mathbf{e}_y are the unit vectors, and ϕ is the relative phase. The synthesized electric field $\mathbf{E}(t, \phi)$ has a trapezoidal envelop, raising linearly during two cycles, then keeping constant for four cycles and decreasing linearly during the last two cycles of the fundamental pulse. At a given time t , the strength of the synthesized

electric field oscillates when the relative phase changes [see Fig. 1(c)],

$$|\mathbf{E}(t, \phi)| = \sqrt{E_x^2 + E_y^2} = |\mathbf{E}_0(t)| + \xi E_1 \cos(2\omega t + \phi) + O(\xi^2), \quad (2)$$

where $|\mathbf{E}_0(t)|$ is the electric field strength of the 800-nm field, $\xi = E_{400}/E_{800}$ is the ratio of the electric amplitudes, and $E_1 = E_{800} \cos(\omega t) / \sqrt{\epsilon^2 \sin^2(\omega t) + \cos^2(\omega t)}$. Because the ionization rate exponentially depends on the electric field strength, the photoelectron yield will change significantly with the relative phase, as shown in Fig. 1(d). For different times, the relative phases where the synthesized electric field strength peaks are different, as shown in Fig. 1(c). Therefore, by monitoring the relative-phase dependence of the photoelectron yield at each momentum in the attoclock experiment, the ionization time could be identified. Noting that in our scheme, the use of the elliptically polarized fundamental field and the perturbative SH field substantially reduces the retrieved ionization time uncertainties resulting from the simultaneous perturbation of the electron trajectories [44]. In our calculations and experiments shown below, the intensity of the SH is 1/6400 of the fundamental field ($\xi = 1/80$), and the uncertainty induced by the SH field is less than 4 as [43]. This is essential for our scheme.

For a given momentum $\mathbf{p} = (p_x, p_y)$, the relation between the relative-phase dependence of the photoelectron yield and the ionization time can be established with the strong-field approximation (SFA) involving the quantum orbitals [45,46], wherein the ionization rate is calculated with exponential accuracy:

$$\Gamma \propto \exp(-2\text{Im}S) = \exp(-2\text{Im}S_0) \exp(-2\text{Im}\Delta S), \quad (3)$$

where

$$S_0(t) = \frac{1}{2} \int_{t_s}^{t_f} dt [p_x + A_x(t)]^2 + \frac{1}{2} \int_{t_s}^{t_f} dt [p_y + A_y(t)]^2 - I_p t_s$$

$$\Delta S(t, \phi) = \int_{t_s}^{t_f} dt [p_x + A_x(t)] \Delta A_x(t, \phi). \quad (4)$$

Here I_p is the ionization potential of the atom, A_x and A_y are the vector potential of fundamental field along the x and y axis, respectively, and ΔA_x is the vector potential of SH. t_f is the ending time of the laser pulse, and $t_s = t_r + it_i$ is the complex transition point [47,48]. Because the intensity of the SH field is several orders of magnitude lower than the fundamental field, we neglect its influence to complex time t_s and keep $\Delta S(t, \phi)$ to the first order of the small quantity ξ . The optimal phase ϕ_Y where the ionization rate maximizes is determined by $\frac{\partial \Gamma}{\partial \phi}|_{\phi_Y} = \frac{\partial \text{Im}\Delta S}{\partial \phi}|_{\phi_Y} = 0$. Then we obtain (see Appendix A for details)

$$\tan(2\omega t_r + \phi_Y) = -\frac{\cosh(2\omega t_i) + 2}{\cosh(2\omega t_i) - 1} \tan(\omega t_r) + \frac{3p_x \omega}{E_{800}} \frac{\cosh(\omega t_i)}{\cosh(2\omega t_i) - 1} \frac{1}{\cos(\omega t_r)}. \quad (5)$$

Thus, by extracting the optimal phase ϕ_Y from the oscillating photoelectron yield at momentum \mathbf{p} , the ionization time t_r can be determined. Note that it requires the imaginary time t_i to retrieve the ionization time.

In particular, for the most probable radial momentum at a given emission angle, Eq. (5) becomes (see Appendix A for details)

$$\tan(2\omega t_r + \phi_Y) = C \tan(\omega t_r), \quad (6)$$

where

$$C = \frac{1}{2} \left\{ 1 - \frac{6\epsilon^2}{a^2} \frac{\cosh(\omega t_i)}{\cosh(2\omega t_i) - 1} \left[\cosh(\omega t_i) - \frac{\sinh(\omega t_i)}{\omega t_i} \right] \right\}. \quad (7)$$

Here, $a = \sqrt{\cos^2(\omega t_r) + \epsilon^2 \sin^2(\omega t_r)}$.

For the linearly polarized field $\epsilon=0$, then $C=1/2$ and Eq. (6) becomes $\tan(2\omega t_r + \phi_Y) = \frac{1}{2} \tan(\omega t_r)$. It is the same as that obtained in Ref. [31]. For the circularly polarized field ($\epsilon = 1$), $a=1$. In the classical limit of $t_i \rightarrow 0$, i.e., $\omega t_i \rightarrow 0$, we have $C=0$ and then Eq. (6) becomes $t_r = -\frac{\phi_Y}{2\omega}$. This result agrees with the prediction of the Ammosov-Delone-Krainov (ADK) formula [49] that for a given ionization instant t_r the photoelectron yield maximizes at the relative phase where the corresponding synthesized electric field $|\mathbf{E}(\phi, t_r)|$ maximizes. For the nearly circular laser field in our calculations ($\epsilon=0.8$), it is still a good approximation that (see Appendix A for details)

$$t_r \approx -\frac{\phi_Y}{2\omega}. \quad (8)$$

This gives a direct relation between the measured optimal phase ϕ_Y and the ionization time t_r for the most probable radial momentum at a given emission angle.

III. RESULTS AND DISCUSSION

We demonstrate our scheme by numerically solving the time-dependent Schrödinger equation (TDSE) [42]. For simplicity, we first consider the model atom with short-range potential $V(\mathbf{r}) = -e^{-r^2}/\sqrt{r^2 + a}$, where $a=0.00116$ is used to match the ground-state energy of helium ($I_p=0.904$ a.u.). Figure 2(a) displays the PEMD initiated by the fundamental field. The intensity and ellipticity of the fundamental field are 3.6×10^{14} W/cm² and 0.8, respectively. It is shown that the PEMD exhibits an elliptical geometry [34,50], and the most probable emission angle θ_{\max} locates at 90° and 270° , which is in agreement with the previous theoretical calculations [21,23,25]. This is more clearly in the radially integrated photoelectron angular distribution (PAD), as shown by the black solid line in Fig. 2(b). To determine the ionization time, we add a perturbative linearly polarized SH field to the fundamental field and scan the relative phase. By monitoring the radially integrated photoelectron yield as a function of the relative phase, we obtain the optimal phase ϕ_Y for different emission angles. The angular-dependent ionization time is determined through Eq. (8) with the extracted optimal phase, as shown in Fig. 2(b). It is shown that the position of the most probable emission angle almost coincides with the time zero (the instant of maximum electric field). This result indicates that the time interval between the ionization instant of the

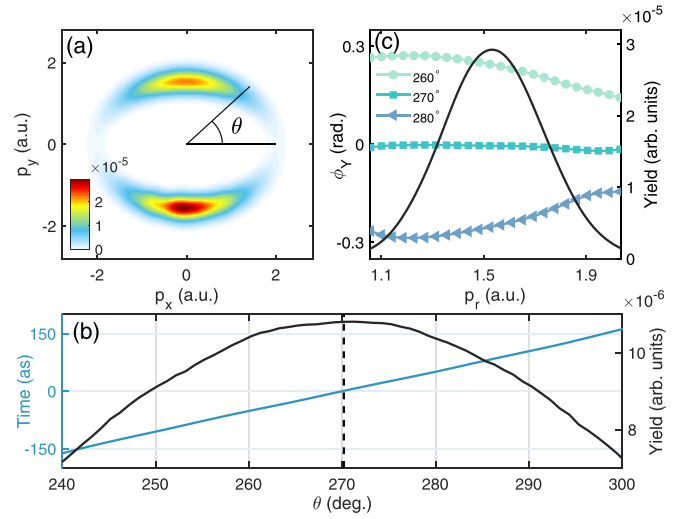


FIG. 2. (a) The calculated PEMD for the strong fundamental field. The model He atoms are ionized in the tunneling regime with a Keldysh parameter $\gamma \approx 0.76$. The electron emission angle θ is defined between the electron emission direction relative to the major axis of the elliptically polarized laser. (b) The retrieved ionization time (blue solid line) with respect to the electron emission angle. The black solid curve and dashed line represent the radially integrated PAD and its peak, respectively. (c) The extracted optimal phase as a function of the electron radial momentum p_r at three emission angles 260° (circles), 270° (squares), and 280° (triangles). The black solid line indicates the radial-momentum distribution of photoelectron at the most probable emission angle 270° .

most probable emission angle and the instant of the maximum field is zero.

With this scheme we further extract the optimal phase ϕ_Y in the full momentum distribution. Figure 2(c) displays the radial-momentum-resolved optimal phase at three emission angles 260° (circles), 270° (squares), and 280° (triangles). The black solid line represents the radial-momentum distribution of photoelectron at the most probable emission angle 270° . It is shown that the optimal phase varies obviously with the electron radial momentum, and the trend of variation depends on the electron emission angle. It is nearly a constant equal to zero at the most probable emission angle $\theta = 270^\circ$. At $\theta = 260^\circ$, the optimal phase decreases as the radial momentum increases, whereas the radial-momentum dependence of the optimal phase is opposite at $\theta = 280^\circ$. These results indicate that the ionization time of photoelectron at a given emission angle depends on the radial momentum.

With the optimal phase ϕ_Y , the ionization time of photoelectrons in the full momentum distribution is obtained utilizing Eq. (5). For the laser parameters in our calculations, the imaginary time t_i is about 12.6 a.u., so we use this value to obtain the ionization time t_r . We mention that the extracted ionization time t_r is not sensitive to the exact value of t_i (see Appendix B for details). Figure 3(a) illustrates the obtained ionization time with respect to the electron radial momentum and the electron emission angle. The radial-momentum dependence of the ionization time can be more clearly observed in Fig. 3(b), which shows the lineouts taken from Fig. 3(a) at the emission angle of 260° (circles), 270° (squares), and 280°

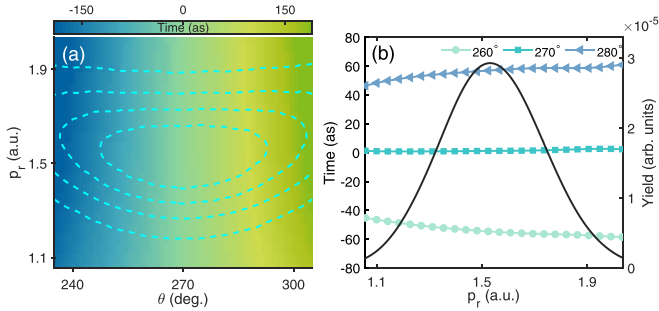


FIG. 3. (a) The retrieved ionization time with respect to the electron radial momentum and the electron emission angle. For comparison, the PEMD in Fig. 2(a) is normalized and displayed by the dashed bright blue contours. Contours correspond to single intensity changing from 0.2 to 0.8 in steps of 0.2, with the innermost contour at 0.8. (b) The lineouts taken at three emission angles 260° (circles), 270° (squares), and 280° (triangles) from (a). The black solid line indicates the radial-momentum distribution of photoelectron at the most probable emission angle 270°.

(triangles). At the most probable emission angle $\theta = 270^\circ$, the ionization time is nearly a constant. It indicates that the ionization time is independent of the radial momentum. Thus the interpretation of the attoclock results with a single value of the offset angle in previous studies is reasonable [21,23,25]. However, at $\theta = 260^\circ$, the ionization time shifts to smaller values as the radial momentum increases, meaning that the electron with larger radial momentum is ionized earlier. At $\theta = 280^\circ$, the situation is reversed.

These results unambiguously indicate that the ionization time depends on the radial momentum and this radial-momentum-resolved ionization time depends on the emission angle. This phenomenon can be understood as follows. For an elliptically polarized laser, the instantaneous direction of the laser vector potential $\mathbf{A}(t)$ and the electric field $\mathbf{E}(t)$ are not perpendicular to each other. It means that there is a nonzero angle $\Delta\alpha$ between the instantaneous vector potential and the initial transverse (transverse to the instantaneous electric field) momentum \mathbf{v}_\perp , as shown in Fig. 4(a). This angle as a function of the ionization time is depicted by the black curve in the inset of Fig. 4(a). The final momentum can be written as $\mathbf{p} = \mathbf{v}_\perp - \mathbf{A}(t_r)$. For a given ionization time t_r , the final momentum \mathbf{p} depends on the magnitude of the initial transverse momentum, as shown schematically in Fig. 4(b). For each ionization time, we calculate the final momentum as a function of the magnitude of the initial transverse momentum. The obtained final momenta at different ionization times are displayed as a series of the colored lines in Fig. 4(c), wherein the orange dashed curve represents the final momentum for $\mathbf{v}_\perp = 0$, i.e., $\mathbf{p} = -\mathbf{A}(t_r)$. To reveal the emission angle dependence of the radial-momentum-resolved ionization time, in Fig. 4(c) we choose three emission angles for demonstration, as indicated by the solid black lines. The line for the emission angle 270° coincides with the colored line for $t_r=0$. It means that the ionization time of photoelectron at the emission angle of 270° is a constant of zero, regardless of its radial momentum. However, it is the different situation for other emission angles. At the emission angle of 260°, it intersects with the colored lines for the earlier ionization time as the radial mo-

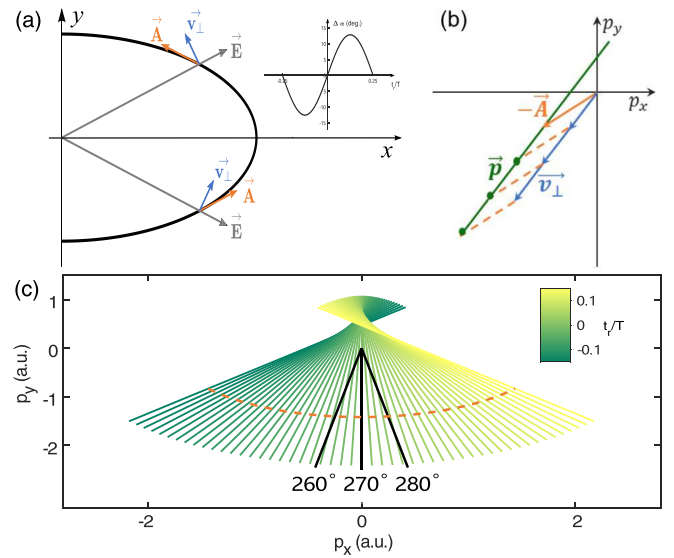


FIG. 4. (a) Sketch of an elliptically polarized laser field. Colored arrows indicate the instantaneous direction of the electric field \mathbf{E} (gray), the laser vector potential \mathbf{A} (orange), and the initial transverse momentum \mathbf{v}_\perp (blue). The inset in the right upper corner presents the ionization time dependence of the angle difference $\Delta\alpha$ between the instantaneous laser vector potential and the initial transverse momentum. Here, T is the optical cycle of the fundamental field. (b) Schematic representation of the electron final momentum distribution, i.e., $\mathbf{p} = \mathbf{v}_\perp - \mathbf{A}(t_r)$ for a given ionization time. (c) The photoelectron final momentum with respect to the ionization time and the initial transverse momentum. Here, the brightness encodes the magnitude of the ionization time. The orange dashed curve expresses the final momentum for $\mathbf{v}_\perp = 0$, i.e., $\mathbf{p} = -\mathbf{A}(t_r)$, and the black solid lines represent three electron emitting angles.

mentum increases. This indicates that at this emission angle the photoelectron with larger radial momentum ionizes earlier. At the emission angle of 280°, it intersects with the colored lines for the latter ionization time as the radial momentum increases. These results demonstrate that the emission angle dependence of the radial-momentum-resolved ionization time shown in Fig. 3 is caused by the initial transverse momentum, or further, the ellipticity of the laser field. Noting that the influence of the ellipticity of the laser field on the offset angle of the attoclock has been discussed in [26,34,51], where several data processing procedures have been proposed to compensate for the ellipticity. Our results show this effect in detail by displaying the ionization time distribution of photoelectron in the full momentum space, which is helpful for understanding the tunneling ionization.

In the attoclock measurements, the long-range Coulomb potential modifies the electron momentum after tunneling and mainly induces the deflection angle in the final momentum distributions. It is difficult to accurately remove the Coulomb effect in previous studies. In our scheme, this task is avoided by introducing the phase-of-the-phase spectroscopy to the attoclock technique [31]. We performed TDSE calculations with model potential of helium atom [$v(r) = -1/(\sqrt{r^2 + 0.0707})$]. The calculated PEMD (without SH field) is shown in Fig. 5(a), where the laser parameters are the same as Fig. 2. It displays that the most probable emission angle locates at

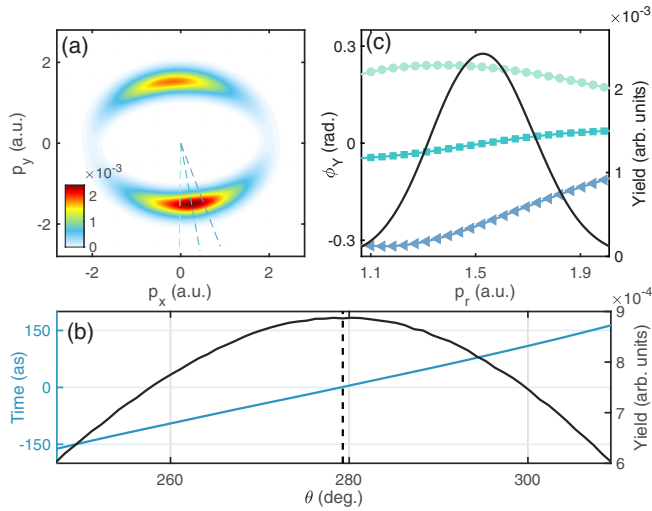


FIG. 5. (a) The PEMD calculated with the model potential for the fundamental field. The laser parameters are the same as Fig. 2. (b) The retrieved ionization time (blue solid line) and the radially integrated PAD (black solid line). The black dashed line indicates the peak of PAD $\theta_{\max} = 279.3^\circ$. (c) The extracted optimal phase ϕ_γ with respect to the electron radial momentum at three emission angles 269.3° (circles), 279.3° (squares), and 289.3° (triangles) [as labeled by the corresponding colored dashed line in (a)]. The black solid line shows the radial-momentum distribution at the most probable emission angle of 279.3° .

$\theta_{\max} = 279.3^\circ$, deviating significantly from the prediction of the SFA model (270°). Using the same scheme, we retrieve the ionization time of different angles, as shown by the blue solid line in Fig. 5(b). By comparing the PAD with the angular-dependent ionization time, we find that the position of the attoclock offset angle coincides with the angle of the zero of ionization time. It indicates that the attoclock offset angle comes entirely from the effect of Coulomb potential, i.e., the tunneling time delay is zero. The result is consistent with several previous experimental measurements by the attoclock technique [16,17,25,31].

In Fig. 5(c), we display the extracted optimal phase at three emission angles 269.3° (circles), 279.3° (squares), and 289.3° (triangles). It is shown that at the most probable emission angle 279.3° , the optimal phase is no longer a constant but changes with the radial momentum. This phenomenon may be caused by the Coulomb interaction. Under the influence of Coulomb potential, the deflection angle of electrons with different energy is different, which further affects the distribution of the ionization time. Furthermore, at $\theta = 269.3^\circ$ and $\theta = 289.3^\circ$, the trends of the optimal phase with electron radial momentum are similar to those of short-range potential. However, the varying ranges of the radial-momentum-resolved optimal phase have changed due to the Coulomb interaction. Therefore the ionization time distribution of photoelectron at a given emission angle is obviously affected. The optimal phase of photoelectron in the full momentum distribution is further shown in Fig. 6(a). Obviously, the optimal phase and thus the corresponding ionization time depends on the radial momentum. At the angles before the most probable emission angle, the optimal phase decreases

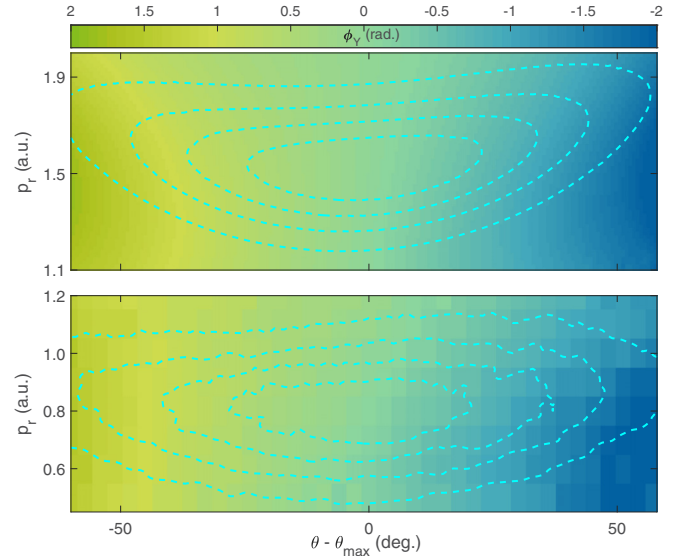


FIG. 6. The extracted optimal phase ϕ_γ from the TDSE calculation of He (a) and the experimental measurement of Ar (b). The dashed bright blue contours represent the corresponding normalized PEMDs. Contours correspond to single intensity changing from 0.2 to 0.8 in steps of 0.2, with the innermost contour at 0.8.

with the radial momentum, while at the angles after the most probable emission angle, it increases with the radial momentum. To confirm this point we performed an experiment with our scheme. In our experiment, the Ar atoms are ionized in the tunneling regime with a Keldysh parameter $\gamma \approx 1.05$ [15,16]. The intensity and ellipticity of the fundamental 800-nm field were calibrated to be $1.2 \times 10^{14} \text{W/cm}^2$ and 0.88, respectively. We measured a series of PEMDs at different relative phases and then extracted the optimal phase with the same procedure as theoretical data (see Appendix C for experimental details). The results extracted from experiments [Fig. 6(b)] agree well with the theoretical results [Fig. 6(a)]. It is worth noting that, in experiments with Ar as the target, in addition to the initial transverse momentum and the Coulomb potential, the multielectron effect and p orbital may affect the radial-momentum dependence of the ionization time.

IV. CONCLUSION

In conclusion, we have unambiguously determined the ionization time of photoelectron in the full momentum distribution. This is achieved by introducing the phase-of-the-phase spectroscopy to the attoclock technique. We demonstrate that the offset angle in the attoclock is entirely induced by the Coulomb potential, confirming the almost zero time delay for the most probable emission angle in the previous attoclock experiments. More importantly, we find that the ionization time of photoelectron significantly depends on radial momentum, and this radial-momentum dependence of the ionization time is closely relevant to electron emission angle. This emission angle dependence of the radial-momentum-resolved ionization time can be traced back to the initial transverse momentum. Besides, the Coulomb potential also affects the

distribution of the ionization time with respect to the electron radial momentum.

ACKNOWLEDGMENTS

This work was supported by the National Key Research and Development Program of China (Grant No. 2019YFA0308300) and the National Natural Science Foundation of China (Grants No. 11874163 and No. 12021004). The computation was completed in the HPC Platform of Huazhong University of Science and Technology.

APPENDIX A: DERIVATION OF EQUATIONS OF THE ARTICLE

The transition rate from the ground state to a continuum state $\mathbf{p} = p_x \mathbf{e}_x + p_y \mathbf{e}_y$ can be estimated with exponential accuracy,

$$\Gamma \propto \exp(-2\text{Im}S) = \exp(-2\text{Im}S_0) \exp(-2\text{Im}\Delta S), \quad (\text{A1})$$

where

$$\begin{aligned} S_0(t) &= \frac{1}{2} \int_{t_s}^{t_f} dt [p_x + A_x(t)]^2 \\ &\quad + \frac{1}{2} \int_{t_s}^{t_f} dt [p_y + A_y(t)]^2 - I_p t_s \\ \Delta S(t, \phi) &= \int_{t_s}^{t_f} dt [p_x + A_x(t)] \Delta A_x(t, \phi). \end{aligned} \quad (\text{A2})$$

Here I_p is the ionization potential of the atom, t_f is the ending time of the laser pulse, and $t_s = t_r + it_i$ is the complex transition point. $A_x(t)$ and $A_y(t)$ are the vector potential of fundamental field along the x and y axis, respectively, and $\Delta A_x(t, \phi)$ is the vector potential of SH, and ϕ is the relative phase. In our study

$$\begin{aligned} A_x(t) &= -\frac{E_{800}}{\omega} \sin(\omega t) \\ A_y(t) &= \frac{\epsilon E_{800}}{\omega} \cos(\omega t) \\ \Delta A_x(t, \phi) &= -\frac{\xi E_{800}}{2\omega} \sin(2\omega t + \phi), \end{aligned} \quad (\text{A3})$$

where E_{800} and ω are the magnitude and frequency of the fundamental 800-nm field, respectively. ϵ is the ellipticity of the fundamental pulse, and ξ is the ratio of the electric amplitudes.

Substituting Eq. (A3) into Eq. (A2), we obtain

$$\begin{aligned} \Delta S(t, \phi) &= \int_{t_s}^{t_f} dt [p_x + A_x(t)] \Delta A_x(t, \phi) \\ &= \int_{t_s}^{t_f} dt \left[p_x - \frac{E_{800}}{\omega} \sin(\omega t) \right] \left[-\frac{\xi E_{800}}{2\omega} \sin(2\omega t + \phi) \right] \\ &= -\frac{\xi E_{800}^2}{12\omega^3} [\sin(3\omega t + \phi) - 3 \sin(\omega t + \phi)] \Big|_{t_s}^{t_f} \\ &\quad + \frac{\xi p_x E_{800}}{4\omega^2} \cos(2\omega t + \phi) \Big|_{t_s}^{t_f}. \end{aligned} \quad (\text{A4})$$

Because the ionization rate is determined by the imaginary part of S , we analyze the imaginary part of $\Delta S(t, \phi)$,

$$\begin{aligned} \text{Im}\Delta S(t, \phi) &= \frac{\xi E_{800}^2}{12\omega^3} [\cos(3\omega t_r + \phi) \sinh(3\omega t_i) \\ &\quad - 3 \cos(\omega t_r + \phi) \sinh(\omega t_i)] \\ &\quad + \frac{\xi p_x E_{800}}{4\omega^2} \sin(2\omega t_r + \phi) \sinh(2\omega t_i). \end{aligned} \quad (\text{A5})$$

For a given ionization time $t_r = \text{Re}(t_s)$, the optimal phase ϕ_Y where the ionization rate maximizes is determined by $\frac{\partial \Gamma}{\partial \phi} |_{\phi_Y} = \frac{\partial \text{Im}\Delta S}{\partial \phi} |_{\phi_Y} = 0$, that is,

$$\begin{aligned} \frac{\partial \text{Im}\Delta S}{\partial \phi} \Big|_{\phi_Y} &= \frac{\xi E_{800}^2}{12\omega^3} [3 \sin(\omega t_r + \phi_Y) \sinh(\omega t_i) \\ &\quad - \sin(3\omega t_r + \phi_Y) \sinh(3\omega t_i)] \\ &\quad + \frac{\xi p_x E_{800}}{4\omega^2} \cos(2\omega t_r + \phi_Y) \sinh(2\omega t_i) \\ &= 0. \end{aligned} \quad (\text{A6})$$

The equation can be further simplified to

$$\begin{aligned} \tan(2\omega t_r + \phi_Y) &= -\frac{\cosh(2\omega t_i) + 2}{\cosh(2\omega t_i) - 1} \tan(\omega t_r) \\ &\quad + \frac{3p_x \omega}{E_{800}} \frac{\cosh(\omega t_i)}{\cosh(2\omega t_i) - 1} \frac{1}{\cos(\omega t_r)}. \end{aligned} \quad (\text{A7})$$

This gives a direct relation between the measured optimal phase ϕ_Y and the tunneling ionization time t_r .

In particular, for the most probable radial momentum at a given emission angle, the x component of the momentum is [52]

$$p_{xm} = \frac{E_{800}}{\omega} \sin(\omega t_r) \cosh(\omega t_i) \left\{ 1 - \frac{\epsilon^2 [\cosh(\omega t_i) - \frac{\sinh(\omega t_i)}{\omega t_i}]}{a^2 \cosh(\omega t_i)} \right\}. \quad (\text{A8})$$

Here $a = \sqrt{\cos^2(\omega t_r) + \epsilon^2 \sin^2(\omega t_r)}$. Substituting Eq. (A8) into Eq. (A7), we obtain

$$\tan(2\omega t_r + \phi_Y) = C \tan(\omega t_r), \quad (\text{A9})$$

where

$$C = \frac{1}{2} \left\{ 1 - \frac{6\epsilon^2}{a^2} \frac{\cosh(\omega t_i)}{\cosh(2\omega t_i) - 1} \left[\cosh(\omega t_i) - \frac{\sinh(\omega t_i)}{\omega t_i} \right] \right\}. \quad (\text{A10})$$

In the classical limit of $t_i \rightarrow 0$, Eq. (A9) becomes

$$\tan(2\omega t_r + \phi_Y) = \frac{1}{2} \left(1 - \frac{\epsilon^2}{a^2} \right) \tan(\omega t_r). \quad (\text{A11})$$

For the circularly polarized field ($\epsilon = 1$), $a=1$, and then Eq. (A11) becomes $t_r = -\frac{\phi_Y}{2\omega}$.

For the nearly circular laser field in our calculations ($\epsilon=0.8$), $t_i = 12.6$ a.u. (see Appendix B below). By numerically solving Eq. (A9), we obtain $t_r = k \frac{\phi_Y}{\omega}$, where the coefficient k is shown in Fig. 7. It displays that the coefficient slightly changes with the ionization time, and it is very close to -0.5 . So approximately, we have $t_r \approx -\frac{\phi_Y}{2\omega}$ for the laser parameters in our paper.

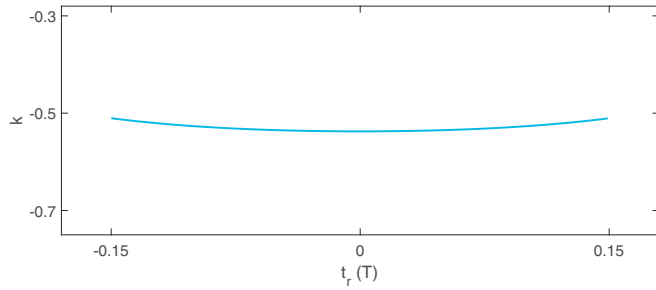


FIG. 7. The coefficient $t_r = k \frac{\phi_Y}{\omega}$ with respect to the ionization time t_r . Here T is the optical cycle of the fundamental field.

APPENDIX B: THE EFFECT OF T_1 ON RETRIEVAL OF THE IONIZATION TIME

In Fig. 7, we show an example of retrieving the ionization time with $t_i = 12.6$ a.u. In fact, the retrieval is not sensitive to the exact value of t_i . Figure 8(a) displays the t_i obtained by solving the saddle-point equation. It is shown that t_i changes slightly in the plane we interested in. We further consider the situation of $t_i = 12.3$ a.u. and $t_i = 14.0$ a.u. Using Eq. (A7) and the extracted optimal phase, the tunneling ionization time are determined, as shown in Figs. 8(b) and 8(c), respectively. It displays that there is no discernible difference between the two results. The t_i dependence of the ionization time can be more clearly observed in Fig. 8(d), which shows the lineouts taken from Fig. 8(b) (dashed lines) and Fig. 8(c) (solid lines) at an emission angle of 260° (blue), 270° (red), and 280° (green). It is shown that the solid lines almost coincide with the dashed lines, indicating that the extracted tunneling ionization time is not sensitive to the exact value of t_i . Thus we treat it as the constant $t_i = 12.6$ a.u., which is the solution of the saddle-point equation for the most probable momentum.

APPENDIX C: EXPERIMENTAL DETAILS

Experimentally, the laser pulse was generated by an amplified Ti:sapphire femtosecond laser system centered at 800 nm and ~ 40 fs duration and a repetition rate of 5 kHz. It was propagated through a $300\text{-}\mu\text{m}$ -thick β -barium borate (β -BBO) crystal to generate the SH. After the BBO, the laser pulses consisted of both fundamental and SH fields. The intensity ratio of the two fields was adjusted by a wire grid polarizer combined with a two-color wave plate. The two-color laser

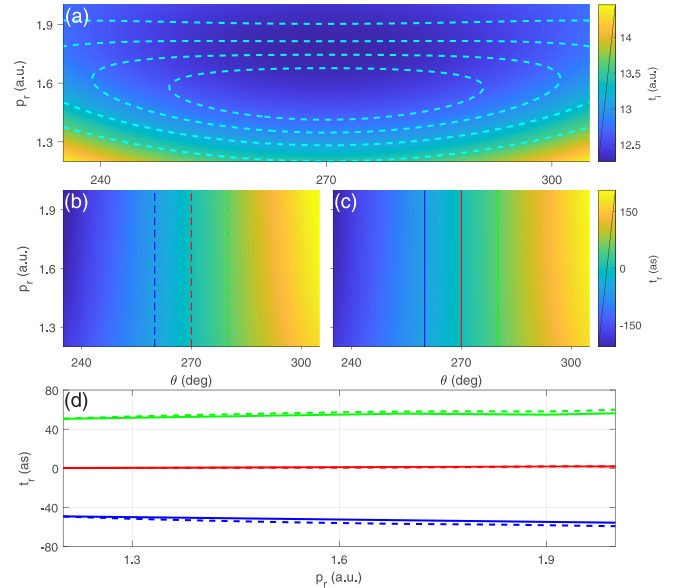


FIG. 8. (a) The distribution of t_i with respect to electron emission angle and electron radial momentum. The dashed bright blue contours represent the normalized PEMD obtained by SFA theory. Contours correspond to single intensity changing from 0.2 to 0.8 in steps of 0.2, with the innermost contour at 0.8. (b, c) The tunneling ionization time determined for Eq. (A7) with $t_i = 12.3$ a.u. (b) and $t_i = 14.0$ a.u. (c). (d) The lineouts taken at the emission angle of 260° (lower blue), 270° (middle red), and 280° (upper green) from (b) (dashed lines) and (c) (solid lines), as labeled by the corresponding colored lines in (b) and (c).

pulse then passed through two dual-order wave plates that change the polarization of the fundamental component while keeping that of the SH component unchanged. The relative phase between the two-color components was controlled by a pair of glass wedges. Then the two-color laser pulse was focused by a parabolic mirror ($f = 75$ mm) onto the jet of argon atoms. The three-dimensional momenta of the ionized photoelectrons were detected using cold target recoil ion momentum spectroscopy (COLTRIMS) [53,54]. The intensity and the ellipticity of the fundamental laser field were calibrated to be 1.2×10^{14} W/cm² and 0.88, respectively. The intensity ratio between the SH and fundamental fields is estimated to be $\sim 1/6400$. More details about the experiment can be found in Ref. [43].

- [1] L. A. MacColl, Note on the transmission and reflection of wave packets by potential barriers, *Phys. Rev.* **40**, 621 (1932).
- [2] A. Fortun, C. Cabrera-Gutiérrez, G. Condon, E. Michon, J. Billy, and D. Guéry-Odelin, Direct Tunneling Delay Time Measurement in an Optical Lattice, *Phys. Rev. Lett.* **117**, 010401 (2016).
- [3] T. Zimmermann, S. Mishra, B. R. Doran, D. F. Gordon, and A. S. Landsman, Tunneling Time and Weak Measurement in Strong Field Ionization, *Phys. Rev. Lett.* **116**, 233603 (2016).

- [4] N. Teeny, E. Yakaboylu, H. Bauke, and C. H. Keitel, Ionization Time and Exit Momentum in Strong-Field Tunnel Ionization, *Phys. Rev. Lett.* **116**, 063003 (2016).
- [5] R. Ramos, D. Spierings, I. Racicot, and A. M. Steinberg, Measurement of the time spent by a tunnelling atom within the barrier region, *Nature (London)* **583**, 529 (2020).
- [6] F. Krausz and M. Ivanov, Attosecond physics, *Rev. Mod. Phys.* **81**, 163 (2009).
- [7] T. Zuo, A. Bandrauk, and P. Corkum, Laser-induced electron diffraction: A new tool for probing ultrafast

- molecular dynamics, *Chem. Phys. Lett.* **259**, 313 (1996).
- [8] M. Lein, N. Hay, R. Velotta, J. P. Marangos, and P. L. Knight, Electron Diffraction in Above-Threshold Ionization of Molecules, *Phys. Rev. Lett.* **88**, 183903 (2002).
- [9] M. Meckel, D. Comtois, D. Zeidler, A. Staudte, D. Pavicic, H. C. Bandulet, H. Pepin, J. C. Kieffer, R. Dörner, D. M. Villeneuve *et al.*, Laser-induced electron tunneling and diffraction, *Science* **320**, 1478 (2008).
- [10] Y. Huismans, A. Rouzée, A. Gijsbertsen, J. Jungmann, A. Smolkowska, P. Logman, F. Lépine, C. Cauchy, S. Zamith, T. Marchenko, J. Bakker, G. Berden, B. Redlich, A. van der Meer, H. Muller, W. Vermin, K. Schafer, M. Spanner, M. Ivanov, O. Smirnova *et al.*, Time-resolved holography with photoelectrons, *Science* **331**, 61 (2011).
- [11] Y. Zhou, O. I. Tolstikhin, and T. Morishita, Near-Forward Rescattering Photoelectron Holography in Strong-Field Ionization: Extraction of the Phase of the Scattering Amplitude, *Phys. Rev. Lett.* **116**, 173001 (2016).
- [12] M. He, Y. Li, Y. Zhou, M. Li, W. Cao, and P. Lu, Direct Visualization of Valence Electron Motion Using Strong-Field Photoelectron Holography, *Phys. Rev. Lett.* **120**, 133204 (2018).
- [13] J. Tan, Y. Zhou, M. He, Y. Chen, Q. Ke, J. Liang, X. Zhu, M. Li, and P. Lu, Determination of the Ionization Time Using Attosecond Photoelectron Interferometry, *Phys. Rev. Lett.* **121**, 253203 (2018).
- [14] Y. Zhou, J. Tan, M. Li, and P. Lu, Probing the launching position of the electron wave packet in molecule strong-field tunneling ionization, *Sci. China: Phys., Mech. Astron.* **64**, 273011 (2021).
- [15] P. Eckle, M. Smolarski, P. Schlup, J. Biegert, A. Staudte, M. Schöffler, H. G. Muller, R. Dörner, and U. Keller, Attosecond angular streaking, *Nat. Phys.* **4**, 565 (2008).
- [16] P. Eckle, A. N. Pfeiffer, C. Cirelli, A. Staudte, R. Dörner, H. G. Muller, M. Büttiker, and U. Keller, Attosecond ionization and tunneling delay time measurements in helium, *Science* **322**, 1525 (2008).
- [17] A. N. Pfeiffer, C. Cirelli, M. Smolarski, D. Dimitrovski, M. Abu-samaha, L. B. Madsen, and U. Keller, Attoclock reveals natural coordinates of the laser-induced tunnelling current flow in atoms, *Nat. Phys.* **8**, 76 (2012).
- [18] I. A. Ivanov and A. S. Kheifets, Strong-field ionization of He by elliptically polarized light in attoclock configuration, *Phys. Rev. A* **89**, 021402(R) (2014).
- [19] A. S. Landsman, M. Weger, J. Maurer, R. Boge, A. Ludwig, S. Heuser, C. Cirelli, L. Gallmann, and U. Keller, Ultrafast resolution of tunneling delay time, *Optica* **1**, 343 (2014).
- [20] A. S. Landsman and U. Keller, Attosecond science and the tunnelling time problem, *Phys. Rep.* **547**, 1 (2015).
- [21] L. Torlina, F. Morales, J. Kaushal, I. Ivanov, A. Kheifets, A. Zielinski, A. Scrinzi, H. G. Muller, S. Sukiasyan, M. Ivanov, and O. Smirnova, Interpreting attoclock measurements of tunnelling times, *Nat. Phys.* **11**, 503 (2015).
- [22] H. Ni, U. Saalmann, and J. M. Rost, Tunneling Ionization Time Resolved by Backpropagation, *Phys. Rev. Lett.* **117**, 023002 (2016).
- [23] A. W. Bray, S. Eckart, and A. S. Kheifets, Keldysh-Rutherford Model for the Attoclock, *Phys. Rev. Lett.* **121**, 123201 (2018).
- [24] M. Han, P. Ge, Y. Fang, X. Yu, Z. Guo, X. Ma, Y. Deng, Q. Gong, and Y. Liu, Unifying Tunneling Pictures of Strong-Field Ionization with an Improved Attoclock, *Phys. Rev. Lett.* **123**, 073201 (2019).
- [25] U. S. Sainadh, H. Xu, X. Wang, A. Atia-Tul-Noor, W. C. Wallace, N. Douguet, A. Bray, I. Ivanov, K. Bartschat, A. Kheifets, R. T. Sang, and I. V. Litvinyuk, Attosecond angular streaking and tunnelling time in atomic hydrogen, *Nature (London)* **568**, 75 (2019).
- [26] C. Hofmann, A. S. Landsman, and U. Keller, Attoclock revisited on electron tunnelling time, *J. Mod. Opt.* **66**, 1052 (2019).
- [27] N. Douguet and K. Bartschat, Attoclock setup with negative ions: A possibility for experimental validation, *Phys. Rev. A* **99**, 023417 (2019).
- [28] W. Quan, V. V. Serov, M. Z. Wei, M. Zhao, Y. Zhou, Y. L. Wang, X. Y. Lai, A. S. Kheifets, and X. J. Liu, Attosecond Molecular Angular Streaking with All-Ionic Fragments Detection, *Phys. Rev. Lett.* **123**, 223204 (2019).
- [29] J. M. Rost and U. Saalmann, Attoclock and tunnelling time, *Nat. Photonics* **13**, 439 (2019).
- [30] V. V. Serov, A. W. Bray, and A. S. Kheifets, Numerical attoclock on atomic and molecular hydrogen, *Phys. Rev. A* **99**, 063428 (2019).
- [31] N. Eicke, S. Brennecke, and M. Lein, Attosecond-Scale Streaking Methods for Strong-Field Ionization by Tailored Fields, *Phys. Rev. Lett.* **124**, 043202 (2020).
- [32] H. Xie, M. Li, S. Luo, Y. Li, Y. Zhou, W. Cao, and P. Lu, Energy-dependent angular shifts in the photoelectron momentum distribution for atoms in elliptically polarized laser pulses, *Phys. Rev. A* **96**, 063421 (2017).
- [33] N. Eicke and M. Lein, Attoclock with counter-rotating bicircular laser fields, *Phys. Rev. A* **99**, 031402(R) (2019).
- [34] C. Hofmann, A. Bray, W. Koch, H. Ni, and N. I. Shvetsov-Shilovski, Quantum battles in attoscience: Tunnelling, *Eur. Phys. J. D* **75**, 208 (2021).
- [35] D. Trabert, N. Anders, S. Brennecke, M. S. Schöffler, T. Jahnke, L. Schmidt, M. Kunitski, M. Lein, R. Dörner, and S. Eckart, Non-Adiabatic Strong Field Ionization of Atomic Hydrogen, *Phys. Rev. Lett.* **127**, 273201 (2021).
- [36] M. Han, P. Ge, J. Wang, Z. Guo, Y. Fang, X. Ma, X. Yu, Y. Deng, H. Wörner, Q. Gong, and Y. Liu, Complete characterization of sub-Coulomb-barrier tunneling with phase-of-phase attoclock, *Nat. Photonics* **15**, 765-771 (2021).
- [37] N. Camus, E. Yakaboylu, L. Fechner, M. Klaiber, M. Laux, Y. Mi, K. Z. Hatsagortsyan, T. Pfeifer, C. H. Keitel, and R. Moshhammer, Experimental Evidence for Quantum Tunneling Time, *Phys. Rev. Lett.* **119**, 023201 (2017).
- [38] S. Skruszewicz, J. Tiggesbäumker, K. H. Meiwes-Broer, M. Arbeiter, T. Fennel, and D. Bauer, Two-Color Strong-Field Photoelectron Spectroscopy and the Phase of the Phase, *Phys. Rev. Lett.* **115**, 043001 (2015).
- [39] M. A. Almajid, M. Zabel, S. Skruszewicz, J. Tiggesbaumker, and D. Bauer, Two-color phase-of-the-phase spectroscopy in the multiphoton regime, *J. Phys. B: At. Mol. Opt. Phys.* **50**, 194001 (2017).
- [40] J. Tan, Y. Li, Y. Zhou, M. He, Y. Chen, M. Li, and P. Lu, Identifying the contributions of multiple-returning recollision orbits in strong-field above-threshold ionization, *Opt. Quantum Electron.* **50**, 57 (2018).
- [41] V. A. Tulskey, M. A. Almajid, and D. Bauer, Two-color phase-of-the-phase spectroscopy with circularly polarized laser pulses, *Phys. Rev. A* **98**, 053433 (2018).

- [42] M. Yu, Y. Zhou, M. Li, and P. Lu, Probing the effect of orbital deformation on the atomic tunneling-ionization-time distribution by phase-of-the-phase spectroscopy, *Phys. Rev. A* **105**, 063103 (2022).
- [43] M. Yu, K. Liu, M. Li, J. Yan, C. Cao, J. Tan, J. Liang, K. Guo, W. Cao, P. Lan, Q. Zhang, Y. Zhou, and P. Lu, Full experimental determination of tunneling time with attosecond-scale streaking method, *Light: Sci. Appl.* **11**, 215 (2022).
- [44] D. Würzler, S. Skruszewicz, A. M. Sayler, D. Zille, M. Möller, P. Wustelt, Y. Zhang, J. Tiggesbäumker, G. G. Paulus, Accurate retrieval of ionization times by means of the phase-of-the-phase spectroscopy, and its limits, *Phys. Rev. A* **101**, 033416 (2020).
- [45] P. Salières, B. Carré, L. Le Déroff, F. Grasbon, G. Paulus, H. Walther, R. Kopold, W. Becker, D. Milošević, A. Sanpera *et al.*, Feynman's path-integral approach for intense-laser-atom interactions, *Science* **292**, 902 (2001).
- [46] W. Becker, F. Grasbon, R. Kopold, D. B. Milošević, G. G. Paulus, and H. Walther, Above-threshold ionization: From classical features to quantum effects, *Adv. At. Mol. Opt. Phys.* **48**, 35 (2002).
- [47] D. B. Milošević, G. Paulus, D. Bauer, and W. Becker, Above-threshold ionization by few-cycle pulses, *J. Phys. B: At. Mol. Opt. Phys.* **39**, R203 (2006).
- [48] T. Yan and D. Bauer, Sub-barrier Coulomb effects on the interference pattern in tunneling-ionization photoelectron spectra, *Phys. Rev. A* **86**, 053403 (2012).
- [49] M. V. Ammosov, N. B. Delone, and V. P. Krainov, Tunnel ionization of complex atoms and atomic ions in electromagnetic field, *Sov. Phys. JETP* **64**, 1191 (1986).
- [50] C. Hofmann, A. S. Landsman, C. Cirelli, A. N. Pfeiffer, and U. Keller, Comparison of different approaches to the longitudinal momentum spread after tunnel ionization, *J. Phys. B: At. Mol. Opt. Phys.* **46**, 125601 (2013).
- [51] N. Eicke and M. Lein, Trajectory-free ionization times in strong-field ionization, *Phys. Rev. A* **97**, 031402(R) (2018).
- [52] S. Luo, M. Li, W. Xie, K. Liu, Y. Feng, B. Du, Y. Zhou, and P. Lu, Exit momentum and instantaneous ionization rate of nonadiabatic tunneling ionization in elliptically polarized laser fields, *Phys. Rev. A* **99**, 053422 (2019).
- [53] R. Dörner, V. Mergel, O. Jagutzki, L. Spielberger, J. Ullrich, R. Moshhammer, and H. Schmidt-Böcking, Cold Target Recoil Ion Momentum Spectroscopy: A 'Momentum Microscope' to View Atomic Collision Dynamic, *Phys. Rep.* **330**, 95 (2000).
- [54] J. Ullrich, R. Moshhammer, A. Dorn, R. Dörner, L. Ph. H. Schmidt, and H. Schmidt-Böcking, Recoil-ion and electron momentum spectroscopy: Reaction-microscopes, *Rep. Prog. Phys.* **66**, 1463 (2003).